

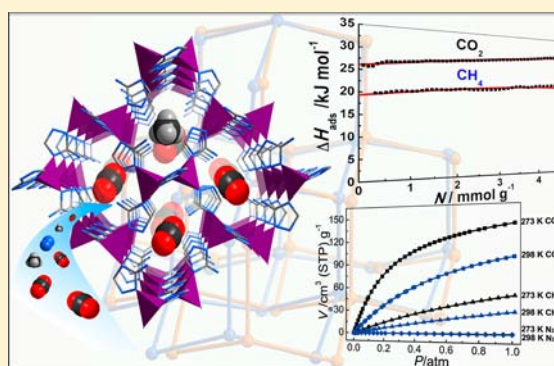
A Zeolite-Like Zinc Triazolate Framework with High Gas Adsorption and Separation Performance

Rui-Biao Lin, Da Chen, Yan-Yong Lin, Jie-Peng Zhang,* and Xiao-Ming Chen

MOE Key Laboratory of Bioinorganic and Synthetic Chemistry, KLGHEI of Environment and Energy Chemistry, School of Chemistry and Chemical Engineering, Sun Yat-Sen University, Guangzhou 510275, China

Supporting Information

ABSTRACT: The reaction of commercially available 3-amino-1,2,4-triazole (Hatz) and $\text{Zn}(\text{OH})_2$ at room temperature produced a porous zeolite-like metal azolate framework, $[\text{Zn}(\text{atz})_2]$ (MAF-66). Single-crystal X-ray diffraction studies of MAF-66 showed that atz^- served as an imidazolate-type ligand, linking tetrahedral Zn^{II} ions to form a noninterpenetrated *dia* framework, which contains a narrow, three-dimensional intersecting channel system (void = 49.8%) functionalized by amino groups and uncoordinated triazolate N atoms on the pore surface. Gas-sorption measurements of MAF-66 revealed high CO_2 uptakes (27.6/19.4 wt % at 273/298 K and 1 atm) and high Henry's law CO_2/N_2 selectivity (403/225 at 273/298 K). The host–guest interactions between CO_2 and the pore surface were also studied by in situ IR absorption spectroscopy and powder X-ray diffraction measurements.



INTRODUCTION

Reversible sorption and energy-efficient capture of CO_2 using physical adsorbents such as porous coordination polymers (PCPs) have attracted great interest for environmental concerns.¹ To enhance the CO_2 adsorption affinity, active sites should be introduced on the pore surface. PCPs with the highest CO_2 uptakes at ambient conditions (~ 1 atm and 298 K) are mostly functionalized with coordinatively unsaturated metal centers (UMCs).² Uncoordinated N donors also have high adsorption affinity for CO_2 .³ Although N donors have weaker activity, their density can be rationally increased without a significant increase of the framework density. Nevertheless, high adsorption affinity (enthalpy) is not always beneficial for practical applications. For example, chemical absorbents have strong interaction with CO_2 , but their poor reversibility and high heat-dissipation requirements make great energy consumption. In fact, the ideal property of an adsorptive material is to have both high adsorption capacity and low adsorption enthalpy.

As a unique type of PCP, zeolitic and zeolite-like metal imidazolate frameworks have received considerable attention in CO_2 capture.⁴ However, compared to other structural types, imidazolate-based frameworks are weak adsorbents for CO_2 because of the lack of active sites (N donors of imidazolate ligands are all coordinated with metal ions; i.e., lone pairs of imidazolate ligands are unavailable for guest species).⁵ Recently, we demonstrated that the 2-methylimidazolate (mim^-) linker in the prototypical zeolitic metal azolate framework SOD- $[\text{Zn}(\text{mim})_2]$ (MAF-4) can be replaced by 3-methyl-1,2,4-triazolate (mtz^-) to give isomorphous SOD- $[\text{Zn}(\text{mtz})_2]$ (MAF-

7) with uncoordinated triazolate N donors exposed on the pore surface, which enhance CO_2 uptakes over 100%.⁵ To further increase the active site density, we used 3-amino-1,2,4-triazolate (atz^-) as an imidazolate-type ligand to construct a new zeolite-like MAF, $[\text{Zn}(\text{atz})_2]$ (MAF-66, **1**), with an interesting structure, high gas uptake, and remarkable gas-adsorption selectivity.

EXPERIMENTAL SECTION

Materials and General Procedures. All reagents and solvents were commercially available and were used without further purification. Elemental analyses (C, H, and N) were performed with a Vario EL elemental analyzer. The phase purity and crystallinity of each product were checked by powder X-ray diffraction (PXRD) using a Bruker D8 ADVANCE powder X-ray diffractometer (Cu $K\alpha$). Thermogravimetric analyses (TGA) were performed using a TA Q50 instrument with a heating rate of 5.0 $^\circ\text{C min}^{-1}$ under a nitrogen atmosphere.

Synthesis. $[\text{Zn}(\text{atz})_2]\cdot\text{guest}$ (**1c**). A solution of 3-amino-1,2,4-triazole (Hatz; 8.68 mmol, 0.730 g) in isopropyl alcohol (iPrOH; 50 mL) was poured into a solution of $\text{Zn}(\text{OH})_2$ (4 mmol, 0.400 g) in aqueous ammonia (25%, 50 mL) and stirred for several minutes. The resultant clear solution was left to evaporate slowly at room temperature. Colorless crystals were collected after 3 days, washed with 3×10 mL of water and then 3×10 mL of iPrOH, and air-dried (0.898 g, yield 85%). Elem. anal. Calcd for $\text{C}_7\text{H}_{15.2}\text{N}_8\text{O}_{1.6}\text{Zn}$ ($[\text{Zn}(\text{atz})_2]\cdot 0.6\text{H}_2\text{O}\cdot 1.0\text{C}_3\text{H}_8\text{O}$): C, 27.80; H, 5.07; N, 37.05. Found: C, 27.83; H, 4.86; N, 37.02.

Received: July 6, 2012

Published: September 6, 2012

$[Zn(atz)_2]_2\cdot guest$ (**1t**). Single crystals: A solution of $Zn(OH)_2$ (0.5 mmol, 0.050 g) in aqueous ammonia (25%, 5.0 mL) was placed on the bottom of a 40 mL test tube, and then benzene (10 mL) was slowly and carefully layered on it, followed by layering of a solution of Hatz (1 mmol, 0.084 g) in 10 mL of ethanol (EtOH). A few colorless polyhedral crystals began to appear after 1 month. Microcrystalline powder: The procedure was similar to that of **1c**, except that methanol (MeOH) was used as the solvent (yield 84%). Elem anal. Calcd for $C_{4.19}H_{13.98}N_{8.03.8}Zn$ ($[Zn(atz)_2]_2\cdot 3.61H_2O\cdot 0.19CH_3OH$): C, 16.63; H, 4.66; N, 37.02. Found: C, 16.62; H, 3.89; N, 37.01.

Single-Crystal X-ray Diffraction Analyses. The diffraction data were collected at 173 K on a Bruker APEX CCD area detector diffractometer (Mo $K\alpha$). Absorption corrections were applied using the multiscan program SADABS.⁶ The structures were solved with direct methods and refined with the full-matrix least-squares technique using the SHELXTL program package.⁷ Because the ligands are highly symmetrically disordered and the space group can only support very limited parameters, only the Zn atom was refined anisotropically in the cubic phase **1c**. We had tried collecting diffraction data for **1c** at lower temperatures, but the diffraction patterns did not change obviously (giving the same unit-cell parameters as those for 173 K). In contrast, all non-H atoms in the tetragonal phase **1t** were refined anisotropically. H atoms were generated geometrically. The atz^- ligands in both structures were constrained to the chemically reasonable geometry. Structural refinement of **1t** is not so good, probably because of the poor crystallinity of the single crystals, or the network structure of this compound may not be fully consistent with the tetragonal symmetry. Crystal data as well as the details of data collection and refinements for the complexes are summarized in Table 1. CCDC 860996 and 860997

Table 1. Crystallographic Parameters of **1c and **1t****

	1c	1t
space group	$Fd\bar{3}m$	$P4_32_12$
a (Å)	13.9429(2)	10.204(2)
c (Å)	13.9429(2)	13.100(2)
V (Å ³)	2710.6(5)	1364.0(3)
Z	192	4
ρ_{calc} (g cm ⁻³)	1.213	1.352
μ (mm ⁻¹)	1.800	1.796
$F(000)$	992	568
Flack parameter x		0.5(2)
R_1^a ($I > 2\sigma$)	0.0758	0.1359
wR_2^b (all data)	0.1777	0.3248
S	1.549	1.074

$$^aR_1 = \sum ||F_o| - |F_c|| / \sum |F_o|. \quad ^b wR_2 = [\sum w(F_o^2 - F_c^2)^2 / \sum w(F_o^2)^2]^{1/2}.$$

contain the supplementary crystallographic data for **1c** and **1t**, respectively. The data can be obtained free of charge from The Cambridge Crystallographic Data Centre via www.ccdc.cam.ac.uk/data_request/cif.

Gas-Sorption Measurements. The sorption isotherms for N_2 , CO_2 , and CH_4 were measured with automatic volumetric adsorption apparatuses (BELSORP-max, BELSORP-HP, and Micromeritics ASAP 2020M). The as-synthesized sample (weight of about 100–200 mg) was placed in the quartz tube and dried for 8 h at 100 °C to remove the remnant solvent molecules prior to measurements. Ultrahigh-purity-grade (99.999%) N_2 , H_2 , CO_2 , and CH_4 were used for all measurements. The temperatures were controlled by a liquid-nitrogen bath (77 K), a liquid-argon bath (87 K), an acetone–dry ice bath (195 K), an ice–water bath (273 K), or a water bath (298 K).

IR Spectroscopy Experiment. The in situ IR absorption spectroscopy measurements of CO_2 adsorption were carried out on a Nicolet/Nexus 670 FT-IR analyzer (2 cm⁻¹ resolution) equipped with a high-temperature cell in mixed N_2/CO_2 flow with a different N_2/CO_2 ratio. The sample powders were gently pressed onto a KBr support, and measurements were performed in the transmission mode.

RESULTS AND DISCUSSION

Synthesis and Structure. Colorless block crystals of **1c** (Figure 1a) were obtained in high yield by the slow evaporation of a clear aqueous ammonia/iPrOH solution of Hatz and $Zn(OH)_2$. A single-crystal X-ray diffraction study showed that **1c** crystallizes in a highly symmetric cubic space group with a very small unit-cell volume [$Fd\bar{3}m$, $Z = 192$, $a = 13.943(2)$ Å, and $V = 2710.6(5)$ Å³], which can only adopt 0.83 non-H atoms in an asymmetric unit, which is much less than the minimum number (3.25; see the Supporting Information) necessary for the description of an ordered structural model for this compound. The structural solution indicated that the asymmetric unit contains one Zn atom (at Wyckoff position 8b with T_d symmetry and $1/24$ occupancy), while no other atom can be directly found in the difference Fourier electron map. Interestingly, the adjacent Zn···Zn distance [6.0375(4) Å] is similar to those of reported zinc(II) imidazolates (ca. 6.0 Å; see Figure S3 in the Supporting Information), indicating that adjacent Zn atoms are bridged by imidazolate-type atz^- ligands. In fact, the diffused electrons in **1c** can be satisfactorily refined as 6-fold disordered atz^- (Figure 1b). The interconnection of adjacent Zn atoms gets a nondistorted **dia** topology (ideal symmetry $Fd\bar{3}m$), which should be only possibly constructed by linear linkers. When a bended imidazolate-type ligand such as atz^- is used, the coordination network must be seriously distorted and have much lower symmetries than the other reported **dia**-type metal imidazolate frameworks (Table S1 in the Supporting Information).^{3b,8} In the refined crystal structure of **1c**, the atomic displacement parameter of the Zn atom is very large (0.179 Å²), which can be understood as the Zn atoms are randomly distributed around the observed, averaged crystallographic sites with small offsets (Figure 1c). This phenomenon indicates that the local coordination geometries in **1c** are not as distorted as that seen from the average structure.

While the structure of **1c** may not be straightforwardly described or understood, we fortunately obtained single crystals of $[Zn(atz)_2]_2\cdot guest$ crystallizing in a tetragonal phase [**1t**, $P4_32_12$, $Z = 8$, $a = 10.201(4)$ Å, $c = 13.082(9)$ Å, $V = 1361(1)$ Å³, and 10 independent non-H atoms] by liquid diffusion between an ethanol solution of Hatz and an aqueous ammonia solution of $Zn(OH)_2$, although the yield and repeatability were very poor. Nevertheless, a microcrystalline powder of **1t** can be efficiently prepared by the slow evaporation of a clear aqueous ammonia/methanol solution of Hatz and $Zn(OH)_2$.

Because the asymmetric unit is large enough, one Zn atom (at Wyckoff position 4a with C_2 symmetry and half-occupancy), one atz^- ligand (general position), and some guest molecules can be directly solved from the single-crystal diffraction data of **1t**. The Zn atom is coordinated by four atz^- ligands to accomplish a distorted tetrahedral geometry [$Zn-N$ 1.88(1)–2.01(1) Å; $N-Zn-N$ 93.7(6)–113.0(5)°]. The triazolate ligand adopts the bended exobidentate coordination mode of imidazolate, using only the 2- and 4-N atoms for coordination, which leaves the 1-N atom uncoordinated. Regarding the Zn atoms as 4-connected nodes and the ligands as linkers, the network topology can be simplified as **dia** (Figure 1d). The noninterpenetrated framework contains three-dimensional channels (void = 49.8%) with a **dia** topology (**dia** is self-dual), having an effective aperture size of 3.2×6.8 Å² and a cavity size of $3.2 \times 4.4 \times 6.8$ Å³. Each amino group forms a

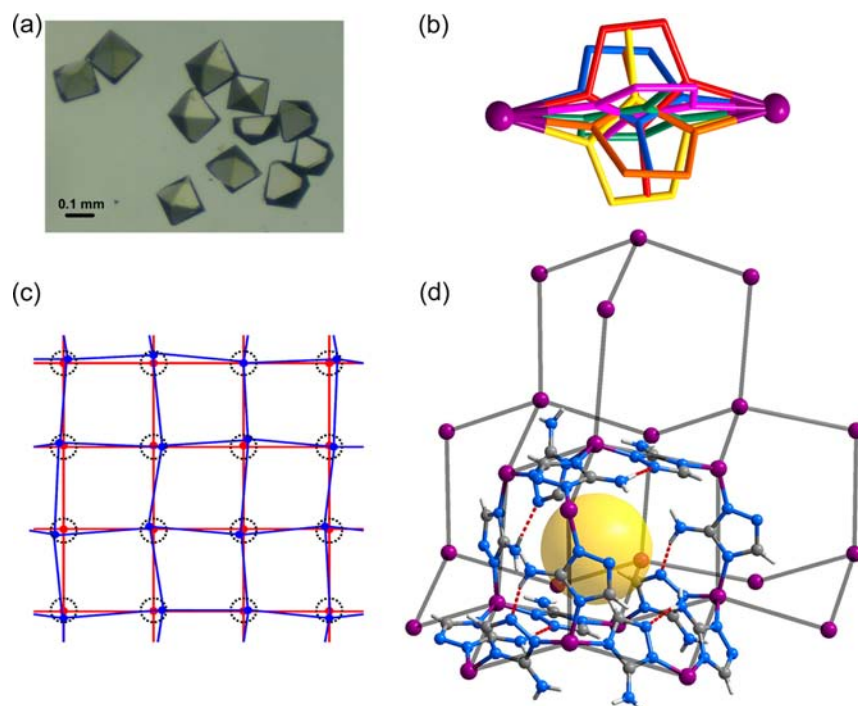


Figure 1. (a) Photograph of single crystals of **1c**. (b) Fragment of **1c** showing two Zn atoms linked by 6-fold disordered atz^- . (c) 2D diagram showing how a nonperiodic network (blue) is observed as a periodic crystal structure (red) with a high degree of disorder (dashed circles: distribution range of the blue nodes around the averaged red ones). (d) **dia** network structure of **1t**.

hydrogen bond with the uncoordinated azolate N atom of an adjacent atz^- ligand [$\text{N}\cdots\text{N}$ 2.77(2) Å; $\text{N}-\text{H}\cdots\text{N}$ 161(1) $^\circ$].

TGA showed that **1c** and **1t** lost all guests molecules at 150–160 $^\circ\text{C}$ and decomposed at ca. 300 $^\circ\text{C}$ (Figures S1 and S2 in the Supporting Information). After guest removal, **1c** and **1t** formed a quasi-amorphous phase (**1a**) with identical PXRD patterns (see Figure S8 in the Supporting Information) and elemental compositions. **1c** and **1t** can also reversibly interconvert to each other by solvent exchange (Figure S8 in the Supporting Information). Finally, considering that **1c** and **1t** were obtained from similar acid–base neutralization reactions between Hatz and $\text{Zn}(\text{OH})_2$ in high yields, we concluded that **1c** and **1t** possess the same **dia**- $[\text{Zn}(\text{atz})_2]$ network structure but with different guest solvent molecules, which leads to different distortions of the frameworks. Compared with the regular/ordered structure **1t**, the complementary active sites (amino groups and triazolate N atoms) in the more amorphous phases **1c** and **1a** should form less and/or weaker hydrogen bonding.

Sorption Properties. The permanent porosity of **1a** was examined by CO_2 and N_2 sorption experiments (Figure 2). The

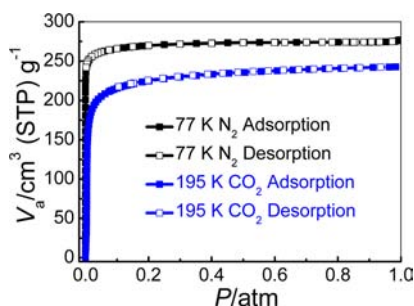


Figure 2. Low-temperature N_2 and CO_2 sorption isotherms for **1a**.

N_2 sorption isotherm at 77 K exhibits a type I character with a saturated adsorption capacity of about 277 cm^3 (STP) g^{-1} , corresponding to a pore volume of 0.43 cm^3 g^{-1} (0.44 cm^3 g^{-1} calculated from the crystal structure **1t**). The Brunauer–Emmett–Teller and Langmuir surface areas were calculated to be 1014 and 1196 m^2 g^{-1} , respectively, which are substantially lower than those of MAF-4 and MAF-7 but still higher than the most open inorganic zeolite (Zeolite Y, 904 m^2 g^{-1}). At 195 K, the saturated adsorption uptake of CO_2 is 243 cm^3 (STP) g^{-1} , corresponding to a pore volume of 0.43 cm^3 g^{-1} identical with that from N_2 measurement and calculated from the crystal structure of **1t**.

The CO_2 uptakes at 1 atm are 140 cm^3 (STP) g^{-1} (6.26 mmol g^{-1} , 27.6 wt %) at 273 K and 99 cm^3 (STP) g^{-1} (4.41 mmol g^{-1} , 19.4 wt %) at 298 K (Figure 3), which are higher than those for most PCPs^{3b,d,e} except a few functionalized with UMCs.² Compared with MAF-4 (no pore surface active site, 5.7 wt % of CO_2 at 273 K) and MAF-7 (density of triazolate N atom 8.7 mmol g^{-1} , 12.3 wt % of CO_2 at 273 K),⁵ the enhanced CO_2 uptakes of **1a** should be attributed to its high density of

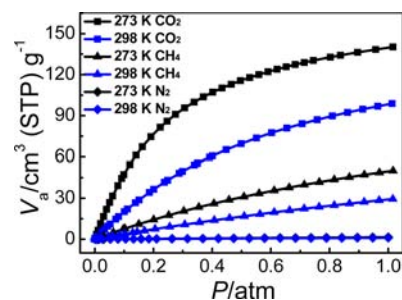


Figure 3. Ambient-temperature CO_2 , CH_4 , and N_2 adsorption isotherms for **1a**.

uncoordinated N atoms (17.3 mmol g^{-1}) on the pore surface and narrow channel size. The **dia** structure of zinc(II) 5-aminotetrazolate^{3b} is isotreticular with **1a** and has an even higher density of uncoordinated N atoms (25.7 mmol g^{-1}), but its CO_2 uptake is obviously lower than that for **1a**. This fact may be ascribed to the much stronger acidity of tetrazole ($pK_a = 4.90$),⁹ making a lower basicity of its uncoordinated N atoms and lower binding affinity to CO_2 , compared with 1,2,4-triazole ($pK_a = 9.97$).⁹

Coverage-dependent CO_2 adsorption enthalpies of **1a** were calculated by both the virial fitting method and Clausius–Clapeyron equation, which agreed well with each other (Figure 4). The enthalpy is 26.0 kJ mol^{-1} at zero coverage,

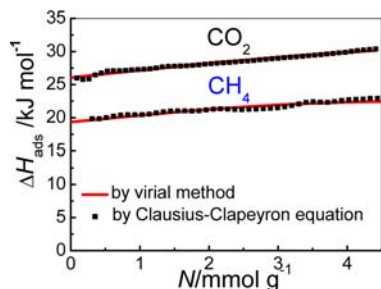


Figure 4. Adsorption enthalpies of CO_2 and CH_4 .

which is lower than those for PCPs functionalized with typical active sites such as UMCs and uncoordinated N atoms ($30\text{--}96 \text{ kJ mol}^{-1}$)^{3e,10} but slightly higher than those for ultramicroporous coordination polymers without active sites ($20\text{--}25 \text{ kJ mol}^{-1}$).^{10a} Considering the very high CO_2 uptake of **1a** at ambient conditions, such low apparent adsorption enthalpy not only is beneficial for reversible adsorption–desorption cycles but also reduces the device requirement for heat transfer.¹¹

It should be noted that the enthalpy monotonically increases along with the loading and reaches 30.2 kJ mol^{-1} at 4.4 mmol g^{-1} , which may be associated with the framework flexibility and/or contribution of guest–guest interactions at high guest loadings. While the phase transition of a highly crystalline host framework is usually reflected by a stepped isotherm and a sudden change of the adsorption enthalpy,¹² the changes of the PXRD pattern and adsorption enthalpy are expected to be much smoother and/or smaller in a quasi-amorphous framework. In situ PXRD patterns of **1a** showed that the main diffraction peak at $2\theta = 11.0^\circ$ ($d = 8.02 \text{ \AA}$) first shifted to 12.9° ($d = 6.84 \text{ \AA}$) and finally to 11.3° ($d = 7.81 \text{ \AA}$), and its intensity obviously increased when the CO_2 pressure increased from 0 to 130 kPa (see Figure S8 in the Supporting Information).

The CH_4 and N_2 uptakes of **1a** at ambient conditions are substantially lower than that for CO_2 . At 1 atm, the adsorption capacity for CH_4 can reach 50.1 and $29.4 \text{ cm}^3 \text{ g}^{-1}$ at 273 and 298 K, respectively, while for N_2 , only 1.5 and $1.0 \text{ cm}^3 \text{ g}^{-1}$ can be adsorbed at 273 and 298 K, respectively. To calculate the adsorption enthalpy at higher CH_4 uptakes, high-pressure sorption isotherms were measured. The uptakes at 20 atm are 142 cm^3 (STP) g^{-1} at 273 K and 116 cm^3 (STP) g^{-1} at 298 K (see Figure S10 in the Supporting Information). Using the high-pressure adsorption data, the enthalpy can be calculated as monotonically increasing from 19.5 kJ mol^{-1} at zero coverage to 22.7 kJ mol^{-1} at 4.4 mmol g^{-1} , indicating an adsorption mechanism similar to that of CO_2 . Compared with CO_2 (quadrupole moment = $1.43 \times 10^{-39} \text{ C m}^2$; polarizability =

$2.63 \times 10^{-24} \text{ cm}^3$),¹³ CH_4 the adsorption enthalpy rises less (3.2 kJ mol^{-1}), which may be due to the relatively weak interaction between low-polarity CH_4 (quadrupole moment = 0 C m^2 ; polarizability = $2.6 \times 10^{-24} \text{ cm}^3$)¹³ and the polar active sites.

Low-pressure H_2 sorption isotherms were also collected. The H_2 uptake for **1a** (2.05 wt % at 1 atm) at 77 K (Figure 5) is

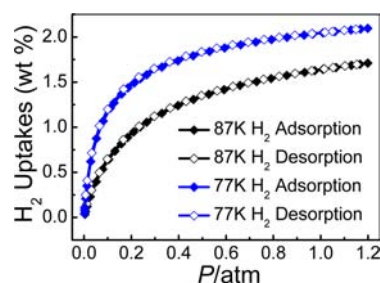


Figure 5. Low-temperature H_2 sorption isotherms for **1a**.

relatively high for PCPs.^{1j,14} Compared with MAF-4 (1.31 wt % of H_2 at 1 atm) and MAF-7 (1.38 wt % of H_2 at 1 atm), the more polar pore surfaces of **1a** can enhance H_2 uptakes.⁵ Coverage-dependent H_2 adsorption enthalpies of **1a** were also evaluated. The zero-coverage enthalpy of 7.0 kJ mol^{-1} is comparable to those of several PCPs with open copper sites.^{1j,14c,15} When the H_2 coverage increases, the enthalpy remains nearly steadily above 6.6 kJ mol^{-1} (Figure 6), which is rare in PCPs.

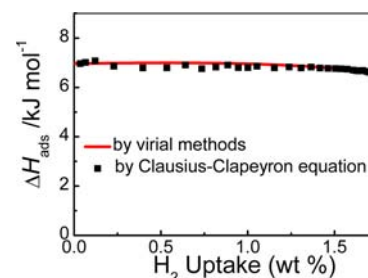


Figure 6. Adsorption enthalpies of H_2 .

Gas Selectivity Studies. The above-mentioned results demonstrated that **1a** has the ability to selectively adsorb CO_2 over CH_4 and N_2 . To estimate the CO_2/CH_4 and CO_2/N_2 adsorption selectivities, the Henry's law selectivity was calculated using the estimated Henry's constants (initial slopes) of single-component adsorption isotherms (see the details in the Supporting Information).¹⁶ On the basis of the above isotherms, the CO_2/CH_4 selectivities of 7.5 and 5.8 were obtained at 273 and 298 K, respectively. Moreover, an ultrahigh CO_2/N_2 selectivity of 403 was obtained at 273 K, which still reaches 225 at 298 K.¹⁶ We also compared the CO_2 and N_2 uptakes at the relevant partial pressures for flue gas (CO_2 0.15 atm; N_2 0.75 atm), which gave CO_2/N_2 selectivities of 282 and 185 at 273 and 298 K, respectively.^{11b} These values, to the best of our knowledge, are significantly higher than the best values for PCPs functionalized with typical active sites such as UMCs and uncoordinated N atoms reported so far^{11b} and only lower than a few chemisorbent-like or highly flexible PCPs.^{17,18} The excellent CO_2 uptake capacity and selectivity of **1a** make it a qualified candidate for CO_2 capture and separation.

IR Studies. To characterize and understand the interactions of CO₂ within the pores of **1a**, we performed in situ IR absorption spectroscopy measurements in mixed N₂/CO₂ flow with different N₂/CO₂ ratios. The spectra obtained after the introduction of CO₂ (0–100%) are shown in Figure 7. Within

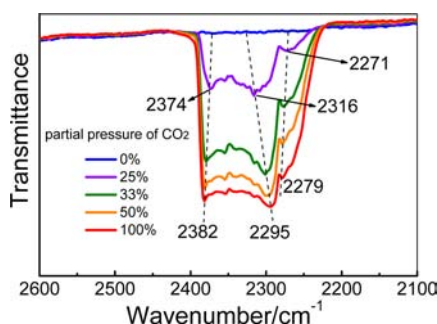


Figure 7. In situ IR absorption spectra of **1a** in mixed CO₂/N₂ flow measured at room temperature.

2400–2200 cm⁻¹, two strong bands at 2382–2374 and 2316–2295 cm⁻¹ (CO₂ asymmetric stretching modes, ν_3) with a shoulder at 2279–2271 cm⁻¹ ($\nu_3 + \nu_2 - \nu_2$ combination mode, hot band) were detected.¹⁹ Compared to the gas-phase single-peak value (2349 cm⁻¹), the splitting peaks with obvious shifts can be associated with two types of adsorbed species (CO₂ molecules) in **1a**. The red-shifted one (from 2316 to 2295 cm⁻¹) indicates that CO₂ acts as an electron acceptor using its C atom to interact with the pore surface, while the blue-shifted ones (from 2374 to 2382 cm⁻¹ and from 2271 to 2279 cm⁻¹) can be assigned to the electron donation through the CO₂ O atoms.²⁰ The gradually increased shifts imply that the interactions between CO₂ and pore surfaces become stronger with higher uptake, which are consistent with the trend of coverage-dependent adsorption enthalpies. These observations may arise from the slight structural changes of the flexible host framework (expose more uncoordinated N atoms and gradually increase the polarity of the pore surface), as suggested by the in situ PXRD measurements.

CONCLUSIONS

In summary, a new zeolite-like, highly porous metal azolate framework functionalized with high-density uncoordinated N donors on the pore surface has been facially prepared by the simple acid–base neutralization reaction using Zn(OH)₂ and a commercially available ligand 3-amino-1,2,4-triazole. Structural analyses, gas-sorption measurements, and IR spectroscopy studies demonstrated that the unique framework and pore surface structures are responsible for its excellent gas uptake capacity and selectivity.

ASSOCIATED CONTENT

Supporting Information

TGA curves, PXRD patterns, additional structural plots, and X-ray crystallographic files in CIF format. These materials are available free of charge via the Internet at <http://pubs.acs.org>.

AUTHOR INFORMATION

Corresponding Author

*E-mail: zhangjp7@mail.sysu.edu.cn.

Notes

The authors declare no competing financial interest.

ACKNOWLEDGMENTS

This work was supported by the “973 Project” (Grant 2012CB821706), National Science Foundation of China (Grants 21121061 and 21001120), and MOE (Grants NCET-10-0863 and ROCS).

REFERENCES

- (a) Chen, S. S.; Chen, M.; Takamizawa, S.; Wang, P.; Lv, G. C.; Sun, W. Y. *Chem. Commun.* **2011**, 47, 4902–4904. (b) Morris, W.; Leung, B.; Furukawa, H.; Yaghi, O. K.; He, N.; Hayashi, H.; Houndonougbo, Y.; Asta, M.; Laird, B. B.; Yaghi, O. M. *J. Am. Chem. Soc.* **2010**, 132, 11006–11008. (c) Chen, Z. X.; Xiang, S. C.; Arman, H. D.; Mondal, J. U.; Li, P.; Zhao, D. Y.; Chen, B. L. *Inorg. Chem.* **2011**, 50, 3442–3446. (d) Bae, Y. S.; Hauser, B. G.; Farha, O. K.; Hupp, J. T.; Snurr, R. Q. *Microporous Mesoporous Mater.* **2011**, 141, 231–235. (e) Zheng, B. S.; Bai, J. F.; Duan, J. G.; Wojtas, L.; Zaworotko, M. J. *J. Am. Chem. Soc.* **2011**, 133, 748–751. (f) Tan, C. R.; Yang, S. H.; Champness, N. R.; Lin, X. A.; Blake, A. J.; Lewis, W.; Schroder, M. *Chem. Commun.* **2011**, 47, 4487–4489. (g) Kim, H.; Kim, Y.; Yoon, M.; Linn, S.; Park, S. M.; Seo, G.; Kim, K. *J. Am. Chem. Soc.* **2010**, 132, 12200–12202. (h) Guo, H. L.; Zhu, G. S.; Hewitt, I. J.; Qiu, S. L. *J. Am. Chem. Soc.* **2009**, 131, 1646. (i) Wang, F.; Tan, Y. X.; Yang, H.; Zhang, H. X.; Kang, Y.; Zhang, J. *Chem. Commun.* **2011**, 47, 5828–5830. (j) Zhuang, W. J.; Yuan, D. Q.; Liu, D. H.; Zhong, C. L.; Li, J. R.; Zhou, H. C. *Chem. Mater.* **2012**, 24, 18–25. (k) Chang, Z.; Zhang, D. S.; Hu, T. L.; Bu, X. H. *Cryst. Growth Des.* **2011**, 11, 2050–2053. (l) Li, J. R.; Tao, Y.; Yu, Q.; Bu, X. H.; Sakamoto, H.; Kitagawa, S. *Chem.—Eur. J.* **2008**, 14, 2771–2776.
- (a) Lee, Y. G.; Moon, H. R.; Cheon, Y. E.; Suh, M. P. *Angew. Chem., Int. Ed.* **2008**, 47, 7741–7745. (b) Wang, Q. M.; Shen, D. M.; Bulow, M.; Lau, M. L.; Deng, S. G.; Fitch, F. R.; Lemcoff, N. O.; Semanscin, J. *Microporous Mesoporous Mater.* **2002**, 55, 217–230. (c) Li, B. Y.; Zhang, Z. J.; Li, Y.; Yao, K. X.; Zhu, Y. H.; Deng, Z. Y.; Yang, F.; Zhou, X. J.; Li, G. H.; Wu, H. H.; Nijem, N.; Chabal, Y. J.; Lai, Z. P.; Han, Y.; Shi, Z.; Feng, S. H.; Li, J. *Angew. Chem., Int. Ed.* **2012**, 51, 1412–1415. (d) Caskey, S. R.; Wong-Foy, A. G.; Matzger, A. J. *J. Am. Chem. Soc.* **2008**, 130, 10870–10871.
- (a) Zhang, S. M.; Chang, Z.; Hu, T. L.; Bu, X. H. *Inorg. Chem.* **2010**, 49, 11581–11586. (b) Panda, T.; Pachfule, P.; Chen, Y. F.; Jiang, J. W.; Banerjee, R. *Chem. Commun.* **2011**, 47, 2011–2013. (c) Burd, S. D.; Ma, S. Q.; Perman, J. A.; Sikora, B. J.; Snurr, R. Q.; Thallapally, P. K.; Tian, J.; Wojtas, L.; Zaworotko, M. J. *J. Am. Chem. Soc.* **2012**, 134, 3663–3666. (d) An, J.; Geib, S. J.; Rosi, N. L. *J. Am. Chem. Soc.* **2010**, 132, 38. (e) McDonald, T. M.; D’Alessandro, D. M.; Krishna, R.; Long, J. R. *Chem. Sci.* **2011**, 2, 2022–2028.
- (a) Phan, A.; Doonan, C. J.; Uribe-Romo, F. J.; Knobler, C. B.; O’Keeffe, M.; Yaghi, O. M. *Acc. Chem. Res.* **2010**, 43, 58–67.
- Zhang, J. P.; Zhu, A. X.; Lin, R. B.; Qi, X. L.; Chen, X. M. *Adv. Mater.* **2011**, 23, 1268.
- Sheldrick, G. M. *SADABS 2.05*; University Göttingen: Göttingen, Germany 2002.
- SHELXTL 6.12*; Bruker Analytical Instrumentation: Madison, WI, 2000.
- (a) Masciocchi, N.; Ardizzone, G. A.; Brenna, S.; Castelli, F.; Galli, S.; Maspero, A.; Sironi, A. *Chem. Commun.* **2003**, 2018–2019. (b) Rettig, S. J.; Sanchez, V.; Storr, A.; Thompson, R. C.; Trotter, J. *J. Chem. Soc., Dalton Trans.* **2000**, 3931–3937. (c) Hayashi, H.; Cote, A. P.; Furukawa, H.; O’Keeffe, M.; Yaghi, O. M. *Nat. Mater.* **2007**, 6, 501–506. (d) Shi, Q.; Chen, Z. F.; Song, Z. W.; Li, J. P.; Dong, J. X. *Angew. Chem., Int. Ed.* **2011**, 50, 672–675.
- Speight, J. G.; Lange, N. A. *Lange’s Handbook of Chemistry*, 16th ed.; McGraw-Hill: New York, 2005.
- (a) D’Alessandro, D. M.; Smit, B.; Long, J. R. *Angew. Chem., Int. Ed.* **2010**, 49, 6058–6082. (b) Vaidhyanathan, R.; Iremonger, S. S.; Shimizu, G. K. H.; Boyd, P. G.; Alavi, S.; Woo, T. K. *Science* **2010**, 330, 650–653.
- (a) Henninger, S. K.; Habib, H. A.; Janiak, C. *J. Am. Chem. Soc.* **2009**, 131, 2776. (b) Sumida, K.; Rogow, D. L.; Mason, J. A.;

McDonald, T. M.; Bloch, E. D.; Herm, Z. R.; Bae, T. H.; Long, J. R. *Chem. Rev.* **2012**, *112*, 724–781.

(12) (a) Stylianou, K. C.; Warren, J. E.; Chong, S. Y.; Rabone, J.; Bacsa, J.; Bradshaw, D.; Rosseinsky, M. J. *Chem. Commun.* **2011**, *47*, 3389–3391. (b) Zhang, J. M.; Wu, H. H.; Emge, T. J.; Li, J. *Chem. Commun.* **2010**, *46*, 9152–9154. (c) Bourrelly, S.; Llewellyn, P. L.; Serre, C.; Millange, F.; Loiseau, T.; Férey, G. *J. Am. Chem. Soc.* **2005**, *127*, 13519–13521. (d) Seo, J.; Matsuda, R.; Sakamoto, H.; Bonneau, C.; Kitagawa, S. *J. Am. Chem. Soc.* **2009**, *131*, 12792–800.

(13) Chowdhury, P.; Bikkina, C.; Gumma, S. *J. Phys. Chem. C* **2009**, *113*, 6616–6621.

(14) (a) Lin, X.; Jia, J. H.; Zhao, X. B.; Thomas, K. M.; Blake, A. J.; Walker, G. S.; Champness, N. R.; Hubberstey, P.; Schroder, M. *Angew. Chem., Int. Ed.* **2006**, *45*, 7358–7364. (b) Liu, Y. L.; Eubank, J. F.; Cairns, A. J.; Eckert, J.; Kravtsov, V. C.; Luebke, R.; Eddaoudi, M. *Angew. Chem., Int. Ed.* **2007**, *46*, 3278–3283. (c) Rowsell, J. L. C.; Yaghi, O. M. *J. Am. Chem. Soc.* **2006**, *128*, 1304–1315.

(15) Ma, S. Q.; Eckert, J.; Forster, P. M.; Yoon, J. W.; Hwang, Y. K.; Chang, J. S.; Collier, C. D.; Parise, J. B.; Zhou, H. C. *J. Am. Chem. Soc.* **2008**, *130*, 15896–15902.

(16) Banerjee, R.; Furukawa, H.; Britt, D.; Knobler, C.; O’Keeffe, M.; Yaghi, O. M. *J. Am. Chem. Soc.* **2009**, *131*, 3875–3877.

(17) McDonald, T. M.; Lee, W. R.; Mason, J. A.; Wiers, B. M.; Hong, C. S.; Long, J. R. *J. Am. Chem. Soc.* **2012**, *134*, 7056–7065.

(18) (a) Liu, X. M.; Lin, R. B.; Zhang, J. P.; Chen, X. M. *Inorg. Chem.* **2012**, *51*, 5686–5692. (b) Zhang, J. M.; Wu, H. H.; Emge, T. J.; Li, J. *Chem. Commun.* **2010**, *46*, 9152–9154. (c) Wu, H. H.; Reali, R. S.; Smith, D. A.; Trachtenberg, M. C.; Li, J. *Chem.—Eur. J.* **2010**, *16*, 13951–13954.

(19) Vimont, A.; Travert, A.; Bazin, P.; Lavalley, J. C.; Daturi, M.; Serre, C.; Férey, G.; Bourrelly, S.; Llewellyn, P. L. *Chem. Commun.* **2007**, 3291–3293.

(20) (a) Duan, J. G.; Yang, Z.; Bai, J. F.; Zheng, B. S.; Li, Y. Z.; Li, S. H. *Chem. Commun.* **2012**, *48*, 3058–3060. (b) Lässig, D.; Lincke, J.; Moellmer, J.; Reichenbach, C.; Moeller, A.; Gläser, R.; Kalies, G.; Cychosz, K. A.; Thommes, M.; Staudt, R.; Krautscheid, H. *Angew. Chem., Int. Ed.* **2011**, *50*, 10344–10348. (c) Luebke, R.; Eubank, J. F.; Cairns, A. J.; Belmabkhout, Y.; Wojtas, L.; Eddaoudi, M. *Chem. Commun.* **2012**, *48*, 1455–1457. (d) Si, X. L.; Jiao, C. L.; Li, F.; Zhang, J.; Wang, S.; Liu, S.; Li, Z. B.; Sun, L. X.; Xu, F.; Gabelica, Z.; Schick, C. *Energy Environ. Sci.* **2011**, *4*, 4522–4527. (e) Wong-Foy, A. G.; Lebel, O.; Matzger, A. J. *J. Am. Chem. Soc.* **2007**, *129*, 15740–15741. (f) Debatin, F.; Thomas, A.; Kelling, A.; Hedin, N.; Bacsik, Z.; Senkovska, I.; Kaskel, S.; Junginger, M.; Müller, H.; Schilde, U.; Jäger, C.; Friedrich, A.; Holdt, H. J. *Angew. Chem., Int. Ed.* **2010**, *49*, 1258–1262.